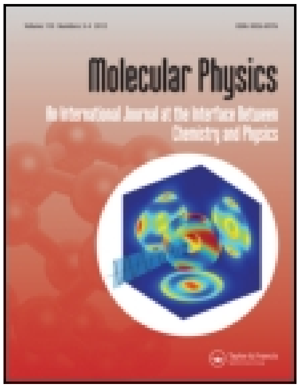

Molecular Physics: An International Journal at the Interface Between Chemistry and Physics
Publication details, including instructions for authors and subscription information:
http://www.tandfonline.com/loi/tmph20

Iodide solvation in tetrahydrofuran clusters: $I^-(THF)_n$ $(1\leq n\leq 30)$

Ryan M. Young [a], R. Julian Azar [a b], Margaret A. Yandell [a], Sarah B. King [a], Martin Head-Gordon [a b] & Daniel M. Neumark [a b]
[a] Department of Chemistry, University of California, Berkeley, CA 94720, USA
[b] Chemical Sciences Division, Lawrence Berkeley National Laboratory, Berkeley, CA 94720, USA

Accepted author version posted online: 05 Apr 2012. Version of record first published: 04 May 2012

To cite this article: Ryan M. Young, R. Julian Azar, Margaret A. Yandell, Sarah B. King, Martin Head-Gordon & Daniel M. Neumark (2012): Iodide solvation in tetrahydrofuran clusters: $I^-(THF)_n$ $(1\leq n\leq 30)$, Molecular Physics: An International Journal at the Interface Between Chemistry and Physics, 110:15-16, 1787-1799

To link to this article: http://dx.doi.org/10.1080/00268976.2012.679637

Molecular Physics
Vol. 110, Nos. 15–16, 10–20 August 2012, 1787–1799

Taylor & Francis
Taylor & Francis Group

INVITED ARTICLE

Iodide solvation in tetrahydrofuran clusters: $I^-(THF)_n$ ($1 \leq n \leq 30$)

Ryan M. Young[a], R. Julian Azar[ab], Margaret A. Yandell[a], Sarah B. King[a], Martin Head-Gordon[ab] and Daniel M. Neumark[ab]*

[a]*Department of Chemistry, University of California, Berkeley, CA 94720, USA;* [b]*Chemical Sciences Division, Lawrence Berkeley National Laboratory, Berkeley, CA 94720, USA*

(*Received 16 February 2012; final version received 16 March 2012*)

The solvent structure and binding motif of iodide-doped tetrahydrofuran clusters, $I^-(THF)_n$ ($1 \leq n \leq 30$) are investigated with anion photoelectron imaging, molecular dynamics simulations, and *ab initio* calculations of vertical detachment energies. Experimentally, a dramatic decrease in the iodide differential stabilization energy and concomitant change in the mass spectrum at $n = 9$ suggest that the first solvation shell closes at $n = 9$–10 THF molecules, in rough agreement with the theoretical result of $n = 7$–9 determined from the computation of relaxed and unrelaxed solvent distribution densities. Analysis of the vertical detachment energy vs. inverse cluster radius suggests the iodide atom is maximally coordinated around $n = 9$. Decomposition of the interaction energies of $I^-(THF)$, its vertically-detached complement, and the $(THF)_2$ dimer, employing the absolutely-localized molecular orbital energy decomposition analysis (ALMO EDA) scheme, highlights the dependence of electron binding and detachment on both electrostatics and polarization, with direct evidence of the fundamental importance of polarizability to a description of detachment. Experimental and theoretical evidence for an anionic electronically excited state is also presented; computed excitation energies and their attendant characters are discussed. The results are interpreted within the framework of the inefficient packing that occurs in bulk neat THF.

Keywords: ion solvation; photoelectron spectroscopy; clusters; charge-dipole interactions

1. Introduction

Ion solvation is a fundamental aspect of chemistry and biology, with broad implications for both natural systems and new materials. The mechanism of solvation and the degree of stabilization are strongly dependent on the structure and properties of both the solvent and solute. To better understand how the solvent structure affects ion solvation, it is advantageous to study a solute with no vibrational or rotational degrees of freedom, such as an atomic ion. Solvated atomic anions such as iodide have served as model systems for ion solvation in bulk solutions for many years [1]. This body of work is complemented by studies of iodide in size-selected clusters [2], at the liquid–vapour interface [3], and in liquid microjets [4]. Experiments on iodide-containing clusters using techniques such as mass spectrometry, photoelectron spectroscopy, and infrared spectroscopy [2,5] have proved particularly valuable as a means of understanding solvation at the microscopic scale, especially when combined with electronic structure and molecular dynamics calculations [6]. These studies yield size- and solvent-dependent energetic and spectroscopic information that provides a window into evolution of solvent structure around the iodide anion with increasing solvation. Here we combine photoelectron imaging spectroscopy with electronic structure calculations to examine the binding energy of iodide in tetrahydrofuran (THF) clusters as a function of size in order to gain insight into how the iodide is solvated within the cluster and over what size range the cluster exhibits a charge-transfer-to-solvent state [7].

Photoelectron spectroscopy has been used to study iodide solvation in large clusters of polar molecules such as water and acetonitrile (CH_3CN). In water, the presence of iodide leads to a large disruption of the hydrogen bond network due to the strong $OH \cdots I^-$ attraction (e.g. 450 meV for iodide to one water molecule) [8]. Size-dependent VDEs from anion photoelectron spectra ($n = 1$–60) [8,9] were originally interpreted as indicating the closure of a solvent shell around $n = 6$, but this inference is not reproduced by molecular dynamics simulations or *ab initio* calculations. For example, calculations by Peslherbe [6] find a surface-bound geometry for clusters as large as $n \sim 55$ where the iodide is coordinated with three or four water molecules; above this size internal solvation becomes favourable. Ultimately, once the iodide is internally solvated it is highly stabilized; photoelectron spectroscopy of iodide in aqueous liquid jets yields a

---

*Corresponding author. Email: dneumark@berkeley.edu

ISSN 0026–8976 print/ISSN 1362–3028 online

http://dx.doi.org/10.1080/00268976.2012.679637
http://www.tandfonline.com

vertical binding energy of 7.7 ± 0.2 eV [4]. This value matches the anion cluster extrapolation quite well (7.92 ± 0.05 eV) [8].

The situation is different for acetonitrile, where photoelectron spectroscopy [10,11] and computational studies [12] suggest the iodide is internally solvated even for clusters as small as $n = 2$. The photoelectron spectra suggest the ion is largely stabilized after $n = 12$, as the vertical detachment energies begin to level out. Molecular dynamics simulations show the electropositive methyl groups are directed toward the halide while the CN groups point outward, allowing for weak hydrogen bonds to form with the second solvent layer. Extrapolation of the cluster photoelectron data [11] indicate that the vertical detachment energy iodide is 8.0 ± 0.2 eV in bulk acetonitrile, a similar stabilization compared to water, despite the much larger dipole moment (3.92 D). As a point of contrast, iodide can also be solvated in a xenon cluster [13–15]. Here, the cluster geometry is determined by spherical packing, resulting in magic numbers in the mass spectrum appearing at sizes with closely-packed geometric structures (I^- is isoelectronic with and similar in size to Xe). Hence the iodide anion is more likely to be internally solvated due to charge-induced dipole interactions. As one might expect, the (extrapolated) stabilization is much less significant in xenon, only about 1.4 eV [13]. The ion has only to disrupt the weak van der Waals interactions between the xenon atoms in order to be incorporated into the cluster.

A weakly polar solvent offers an intermediate case between a rare gas and strongly polar solvent molecules like water or acetonitrile. Tetrahydrofuran (THF, C_4H_8O) is weakly polar in that it has a sizeable dipole moment (1.63–1.75 D) but a relatively small static dielectric constant ($\varepsilon_s \sim 7.5$). Neat THF has been shown to pack inefficiently, indicating a weaker solvent-solvent interaction. Mixed quantum/classical molecular dynamics simulations [16] and neutron scattering experiments [17] have shown that neat THF has large voids, ~2.5–5 Å atom-to-atom, which are positively polarized. This result has important implications for electron and ion solvation, as these voids may act as pre-existing traps for solvation of a negative ion or electron with little nuclear rearrangement. Transient absorption experiments show that after an excess electron is injected or excited using a femtosecond pulse, it appears with its equilibrated absorption spectrum within the time-resolution of the experiment, consistent with injecting an electron into a pre-formed cavity [18,19].

This solvent structure might also be expected for neutral THF clusters of sufficient size, where the voids would act as favorable binding sites for excess electrons. Photoelectron spectra of $(THF)_n^-$ clusters [20] suggest that clusters as small as $n = 6$ can support a solvated electron; the VDE of this cluster is about 2 eV, significantly higher than in comparably-sized water cluster anions. Extrapolation to infinite cluster size yields a bulk binding energy of about 3.1 eV, in agreement with the photoelectron spectroscopy of electrons solvated in liquid THF jets [21]. The bulk value lies only 1 eV higher than the VDE of $(THF)_6^-$. This low stabilization energy and large binding energy for small cluster anions together suggest that the solvent cluster readily accepts the excess electron even at small sizes. Given its effect on electron solvation, the effect of this frustrated packing on the location and degree of stabilization of iodide in $I^-(THF)_n$ clusters is an interesting question, specifically how the ion is stabilized as a function of cluster size.

Here we study iodide solvation in THF clusters using a combination of anion photoelectron spectroscopy and molecular dynamics/electronic structure calculations. The photoelectron spectra yield size-dependent VDEs of $I^-(THF)_n$ clusters up to $n = 30$, and show a significant drop in the differential stabilization energy above $n = 9$. Such a result suggests that the $n = 9$ cluster has a complete solvent shell around the iodide core, but such an inference may be simplistic in light of previous work on other iodide-solvent clusters. To explore this result further, the question of solvation structure is addressed computationally by determining the so-called solvent distribution density. This is a measure of the probability of finding a solvent molecule at a given radial distance from the iodide atom, given an ensemble of minimum-energy cluster configurations obtained by molecular dynamics simulations, thus allowing for the trivial computation of coordination number, as well as the radial extent and character of the primary and secondary solvation layers. We find from the probability distribution functions and detachment energy profile information a partial closing of the first solvation shell between 7 and 9 THF molecules. We also present experimental and theoretical evidence for an autodetaching electronic excited state beginning at $n = 4$ and discuss the nature of the excitation with the aid of excited state calculations.

2. Methods

2.1. *Experimental methods*

The photoelectron imaging apparatus has been described in detail previously [22]. Briefly, argon gas at 20–40 psig was flowed over reservoirs of THF and methyl iodide, co-expanded through a 100 Hz pulsed solenoid valve [23], and intersected with ~500 eV electrons from a ring anode. Secondary electron attachment led to dissociative electron attachment to CH_3I, forming free I^- which could either be captured by neutral THF clusters or act as a nucleation site for the formation of $I^-(THF)_n$. These clusters were extracted perpendicularly into a Wiley–McLaren time-of-flight mass spectrometer [24] allowing for size-selection. Mass spectra were collected and integrated using a digital oscilloscope (Tektronix DPO3034C). To obtain photoelectron spectra, selected masses were interrogated by the appropriate laser pulse and ejected electrons were analyzed using velocity map imaging [25]. Collected images were transformed using the BASEX method [26], reconstructing the molecular frame kinetic energy distribution. The electron kinetic energy (eKE) is transformed into electron binding energy (eBE) by conservation of energy: $eBE = h\nu - eKE$. The photoelectron spectrometer was calibrated against I^- detachment to ensure the proper electron affinity (3.059038 eV) [27] of atomic iodine and the spin-orbit splitting (0.943 eV) between its $^2P_{3/2}$ and $^2P_{1/2}$ states. The laser wavelength was measured using a fibre-optic spectrometer (Ocean Optics USB2000 + XR1). Photoelectron angular distributions were also obtained but are not reported here.

Laser pulses were generated using a commercial Ti:sapphire femtosecond oscillator and chirped-pulse multipass amplifier (KM Labs Griffin oscillator/Dragon amplifier) resulting in 35 fs FWHM pulses at 790 nm (1.57 eV). 1 mJ of this output was used to pump a continuum-seeded optical parametric amplifier (Light Conversion TOPAS-C). Ultraviolet photons at 239 nm (5.19 eV) were generated by second harmonic generation of the sum-frequency signal OPA output in a β-barium borate (BBO) crystal at 56°, while the 290 nm – 320 nm (4.28 eV – 3.88 eV) excitation pulses were generated by doubling the sum-frequency idler output using a 40.5° BBO crystal.

2.2. *Computational methods*

All *ab initio* calculations were performed using a developmental version of the Q-Chem software package [28]. Gas-phase vertical detachment energies (VDEs) are given by the (non-zero-point-corrected) vertical energy difference between the Born–Oppenheimer singlet and doublet surfaces corresponding to the anionic and neutral species, respectively:

$$VDE = E\left(\left|\Phi_{q=0,M_s=1/2}\right\rangle\right)\Big|_{\text{anion geom}} - E\left(\left|\Phi_{q=-1,M_s=0}\right\rangle\right)\Big|_{\text{anion geom}} \quad (1)$$

Koopmans' ionization potentials (IPs) are also computed from the HOMO orbital eigenvalue of the anionic Hartree–Fock wavefunction,

$$IP = -\varepsilon_{HOMO}. \quad (2)$$

VDEs were evaluated for $I^-(THF)_n$ clusters using both wave function and density functional theory (DFT) methods. For DFT calculations of VDEs, we chose to employ the B3LYP [29] and PBE [30] functionals, based on test calculations comparing against wave function methods for the $n = 1$ complex. With respect to atomic orbital basis sets, the THF molecules are treated in the 6–31++G** basis (containing a single set of polarization and diffuse functions on the heavy atoms), while for iodide we employed the 'small-core' aug-cc-pVTZ-PP basis set [31], which has sufficient diffusivity to adequately describe the iodide 5p orbitals. (The $n = 4$ and 5 principal shell electrons are treated explicitly, while the core electrons are treated with a scalar relativistic effective core potential.)

To investigate the character of the excited state and the autodetachment feature presented in Section 3, TD-DFT [32] ωB97X-D calculations within the Tamm–Dancoff approximation [33] were performed on the $n = 4$ ensemble of structures, to obtain the lowest excited-state roots of singlet multiplicity. The frontier orbitals were visualized at a contour value of $0.01\,\text{Å}^{-3/2}$. Standard density functionals furnish an incorrect large-r Coulomb tail due to the well-known self-interaction problem, and thus, diffuse or Rydberg states, which rely heavily on a correct large-r inter-electronic potential, are described incorrectly [34]. The so-called 'long-range-corrected' ωB97 suite of exchange-correlation functionals [35,36] guarantees full Hartree–Fock exchange at large inter-electronic distances, as necessary to treat charge-transfer and Rydberg-like excited states, and so is preferred in this study over the B3LYP functional.

Nuclear geometries for the *ab initio* calculations were obtained as snapshots collected along molecular dynamics trajectories that were performed for each cluster size for 100 ps. After a 50 ps equilibration period, geometry snapshots were harvested every 2 ps. These molecular dynamics simulations were performed using the TINKER molecular modeling package [37] employing the AMOEBA polarizable atomic multipole force field [38] at 100 K (the estimated experimental temperature). AMOEBA parameters for THF were not directly available, but parameters are available for the isoelectronic five-membered ring pyrolidine (tetrahydropyrrole), which has a very similar equilibrium structure [39]. Bonded and non-bonded parameters for C and H were taken directly from pyrolidine, while those for O were taken from dimethyl ether. Dihedral parameters were also taken from pyrolidine. The inclusion of polarizability in the force field, as explored previously for $Cl^-(H_2O)_n$ clusters [40] and $I^-(CH_3CN)_n$ clusters [11], is expected to be very important for a correct description of the THF-iodide interactions. As full relaxation of the geometries collected via the snapshots is not readily feasible using *ab initio* calculations, the results obtained rely on the AMOEBA force field being a reasonably accurate approximation. This will be directly validated for small clusters.

The snapshot independence within a trajectory was assessed by calculation of the velocity autocorrelation (VAC) function for the x-component of the I^- atom's velocity vector across all cluster sizes:

$$C_v(t) = \langle v_x(0)v_x(t)\rangle / \langle v_x(0)\rangle^2 \tag{3}$$

where the angled brackets denote a time average.

The VAC generally decayed to a thousandth of its initial value by $t \sim 1.25$ ps, which is the basis for harvesting geometry snapshots from the AMOEBA trajectories at 2 ps intervals, with the objective of obtaining uncorrelated geometries. One can also consider this choice of snapshot interval by looking at cluster normal modes. The 'hardest' intramolecular vibrations, of energies between 2000 and 3000 cm^{-1}, have periods between ~10 and ~20 fs, while the 'softest', primarily intermolecular vibrations of energies between ~50 and ~100 cm^{-1}, have periods between ~300 and ~600 fs. Both period time intervals are much smaller than the equilibration time, and somewhat smaller than the snapshot interval.

Based on the snapshots from the AMOEBA trajectories, VDEs were directly computed by the *ab initio* methods discussed above to define 'unrelaxed' VDEs. Additionally, so-called 'relaxed' detachment energies were computed at geometries derived from the snap-shots by minimizing the nuclear forces on the AMOEBA potential surface. The maximum standard error of the mean for a detachment/excitation energy distribution obtained in this study was roughly ±15 meV.

The solvation structure of the clusters was investigated by computing the solvent radial density, $D(r)$, defined as the number of THF centres of mass found in a shell of volume $4\pi r^2 dr$ at a distance r from the iodide,

$$D(r) = \frac{1}{N}\langle n(r)\rangle \tag{4}$$

where N is the number of solvent molecules and the bracketed quantity is the time average of the number of solvent molecules at a given displacement r.

$$\langle n(r)\rangle = \frac{1}{N}\sum_{i}^{N_t} n_i(r) \tag{5}$$

In practice, $D(r)$ was evaluated from the trajectories by binning the centres of mass into intervals of 0.05 Å. The computed $D(r)$ can be integrated to give the number of solvent molecules within selected limits of integration; intervals of significant intensity will serve to delineate distinctive solvation layers about the iodide. It should be mentioned that calculated solvent distribution densities and electron detachment profiles, at least in the low-n limit, are for the most part, relatively temperature-insensitive, a result confirmed in the supplementary material for $T = 200$ K presented in Figure S.1 in the Supplementary material (a rough upper bound to the estimated experimental temperature).

The question of surface versus bulk solvation of iodide in THF is addressed by computing the radius of gyration for the THF cluster, given as the root mean square deviation of the solvent molecule positions from the cluster centre of mass,

$$R(t)^2 = \frac{1}{N_t}\sum_{i}^{N_i} (r_i(t) - r_{COM}(t))^2 \tag{6}$$

This is compared with the magnitude of the separation of the iodide with respect to the cluster centre of mass, $|r_I - r_{COM}|$. Taken together, these quantities give a picture of the iodide displacement from the averaged, finite-volume centre of the solvent cluster at a given time.

Solute-solvent interaction energies were investigated using an energy decomposition analysis (EDA) from an absolutely-localized molecular orbital (ALMO) reference [41,42]. The ALMO-EDA is a successful [43–46] scheme that variationally separates physically relevant components of intermolecular interactions by imposing the condition on the DFT minimization that molecular orbitals on a given fragment include contributions only from atomic orbitals on that fragment. The decomposition components include: (i) frozen orbital interactions, accounting for both permanent electrostatic contributions and Pauli repulsions between filled orbitals, as obtained by bringing non-interacting distorted molecules together to form an antisymmetrized product of fragment wavefunctions; (ii) polarization, the *intra*molecular relaxation of fragment ALMOs in the field of all other ALMOs on other fragments; and (iii) charge transfer, the stabilization due to *inter*molecular (delocalized) relaxation of molecular orbitals in occupied-virtual pair interactions. The sum of these terms gives the total DFT binding energy,

$$\Delta E_{bind} = \Delta E_{frz} + \Delta E_{pol} + \Delta E_{CT} \tag{7}$$

and as such, the ALMO-EDA can yield insight into the complicated interplay of forces stabilizing weak interactions. We expect this decomposition to be a useful tool in the quantification of the elements stabilizing solute–solvent and solute–solute interactions, presumably dominated by frozen electrostatics, and strongly affected by the relative positions and orientations in the cluster. All geometries for ALMO EDA calculations were obtained at the B3LYP/6-31++G** level with the aug-cc-pVTZ-PP basis for the iodine atom. Benchmark optimizations on the binary I^-(THF) complex were performed with the aug-cc-pVDZ-PP basis on iodide and the 6–31 G* basis on THF.

3. Results and analysis

3.1. *Mass spectrum*

Figure 1 shows a representative mass spectrum produced from the gas mixture and ion source described in Section 2.1. Iodide dominates the spectrum at $m/z = 127$ with clustering occurring every 72 mass units, indicative of $I^-(THF)_n$ cluster formation. The shape of the mass spectrum is not constant or monotonic with cluster size: signal for clusters up to $n \sim 10$ are more intense than for $n > 10$, after which the distribution is more or less constant until single-cluster resolution is lost around $m/z \sim 4000$. While altering the source conditions always leads to changes in the mass spectrum, the relative enhancement of the first ten peaks to the larger sizes is always seen. The inset of Figure 1 shows the first 15 clusters, highlighting this trend. Contamination from I_2^- is seen at small cluster sizes, but the mass resolution of the spectrometer is sufficient ($\Delta m/m \sim 1\%$) to isolate the desired clusters. Moreover, solvated I_2^- is spectroscopically distinct from atomic iodide and is not observed in any of the photoelectron spectra.

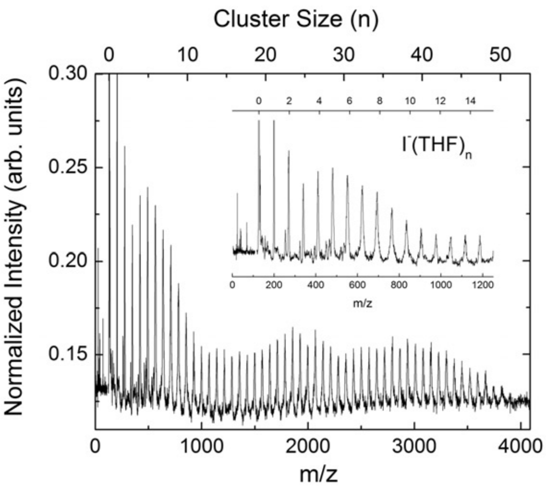

Figure 1. Time-of-flight mass spectrum of $I^-(THF)_n$ clusters showing cluster production out to $n \sim 55$. Inset: zoom in on first 12 clusters, showing a change in intensity at $n = 9$–10.

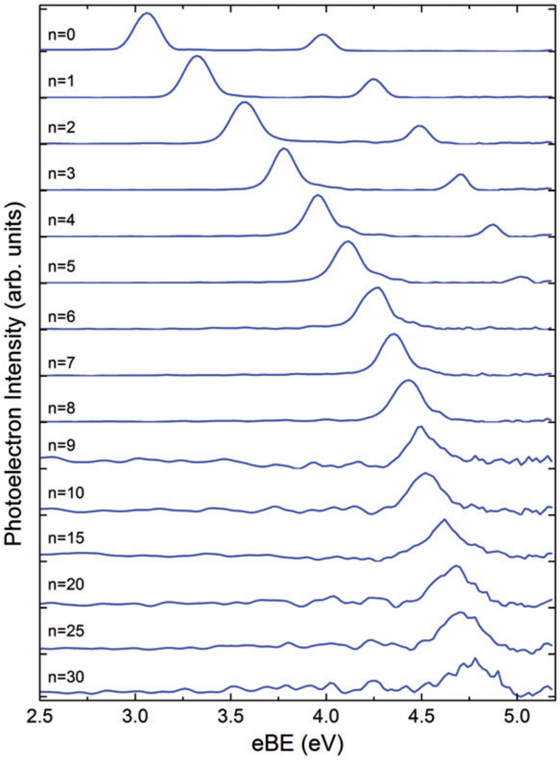

Figure 2. Photoelectron spectra of selected $I^-(THF)_n$ ($0 \le n \le 30$) clusters at 5.19 eV photon energy.

3.2. *Photoelectron spectra*

Photoelectron spectra are shown in Figure 2 for various sizes up to $n = 30$ using a photon energy of 5.19 eV. Detachment from solvated iodide shows the characteristic spin-orbit structure in the photoelectron spectrum of I^-, shifting to higher binding energies until $n = 6$ when only detachment to the $^2P_{3/2}$ state of solvated neutral iodine is energetically possible. For all sizes studied here, the vertical detachment energy of the cluster is determined by subtracting the centre of a Gaussian fit to the eKE distribution of the $^2P_{3/2}$ peak $[E_0(n)]$ from the photon energy: $VDE(n) = h\nu - E_0(n)$. The stabilization energy for a given cluster is computed as

$$E_{stab}(n) = VDE(n) - EA\left[I\left(^2P_{3/2}\right)\right]. \tag{8}$$

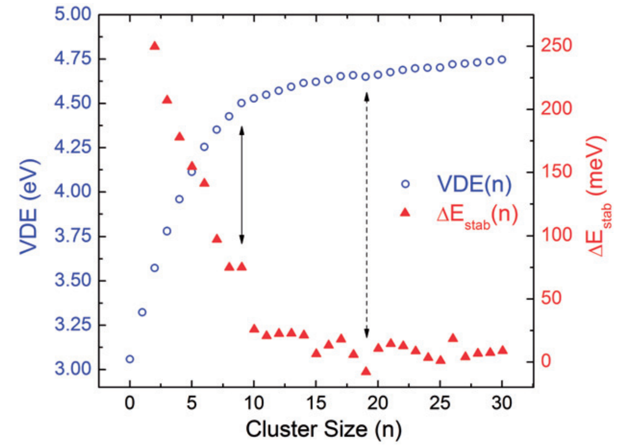

Figure 3. VDE vs. cluster size (n) for $I^-(THF)_n$ ($0 \leq n \leq 30$), (blue circles) is presented on the left axis, with differential stabilization energy, $\Delta E_{stab}(n) = E_{stab}(n) - E_{stab}(n-1)$ (red triangles), presented on the right axis. The left arrow marks the change at $n = 9$, while the right arrow marks the onset of the long-range interactions.

The differential stabilization energy, the amount by which the excess charge is stabilized for one cluster size relative to the one unit smaller, is defined as:

$$\Delta E_{stab}(n) = VDE(n) - VDE(n-1), \qquad (9)$$

effectively the slope of the VDE vs. n plot. These are shown along with the VDEs in Figure 3. The left ordinate shows the VDE while the right shows the differential stabilization energy. VDEs are seen to monotonically increase with cluster size. The rise is steep until $n = 9$ when the VDEs begin to increase more slowly. This change is mirrored in the differential stabilization energies as well: these remain positive for most sizes but are significantly smaller for $n > 9$.

Varying the photon energy has a marked effect on the shape of the photoelectron spectra for certain sizes. Figure 4 shows PE spectra of the $n = 4$ cluster at two different photon energies: $h\nu = 4.05$ eV and $h\nu = 5.19$ eV [VDE($n = 4$) = 3.96 eV]. Direct detachment (Feature A) is observed with both photon energies, while the sharp peak (Feature B) is seen only at 4.05 eV, close to the VDE of the cluster. Feature B comprises very low eKE electrons and is characteristic of excited state autodetachment, which can be seen only when the excitation laser is resonant with an anionic excited state [47–49]. This feature is observed in the photoelectron spectra for $n = 4$–7, narrowing with increasing cluster size when the photon energy is tuned to be on resonance (the autodetachment feature is most intense for a given cluster size and set of clustering/ionization conditions). By $n = 8$, no autodetachment feature was observed while pumping the cluster below and around the detachment threshold.

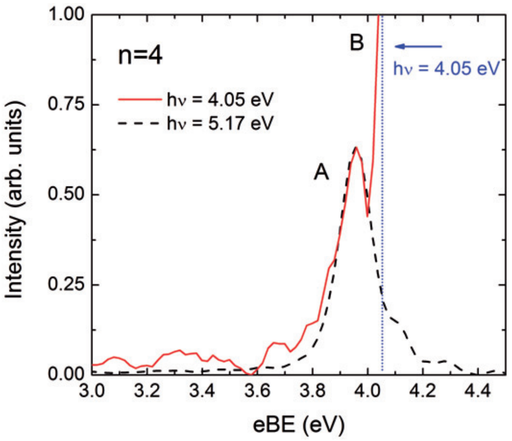

Figure 4. Photoelectron spectrum of $n = 4$ taken at 4.05 eV (red solid line) and 5.19 eV (dashed black line) photon energies, showing direct ground-state detachment (Feature A) as well as a narrow, intense feature at low kinetic energy, characteristic of excited state autodetachment (Feature B). The vertical blue dotted line marks the highest binding energy accessible by the 4.05 eV photons.

3.3. *Computational results*

Velocity autocorrelation (VAC) functions for the iodide anion in $n = 1$, 4, 5 and 10 clusters are shown in Figure 5. For $n = 1$,4, the VAC shows clear recurrences (with period ~300 fs) that resemble motion in a local harmonic potential. For $n = 5$–14, the VAC is broader and with hindered recurrences, as more frequent collisions with solvent molecules change the direction of the ion's momentum vector. The result is stronger damping of the VAC with time, or in other words, a shorter 'memory' of iodide for its initial velocity.

We performed two validations of the quality of the geometries obtained as snap-shots from the classical trajectories propagated on the AMOEBA potential energy surface. First, we explicitly optimized the $I^-(THF)$ complex at various levels of *ab initio* theory, and compared the interatomic distance $|r_O - r_I|$ and the O-αC-I orientation angle against the values obtained with the AMOEBA force field. These values are compiled in Table S.1. AMOEBA gives a $|r_O - r_I|$ distance and ∠O-αC-I of (5.84 Å, 114°), as compared to the PBE (DFT) results of (5.62 Å; 123°), B3LYP (DFT) results of (5.61 Å, 123°), and wave function-based MP2 results of (5.32 Å; 126°). While not in

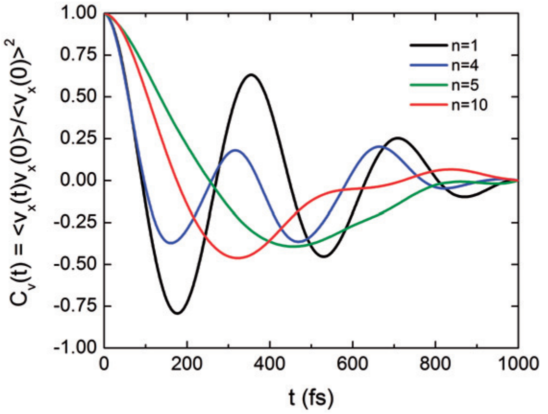

Figure 5. Velocity autocorrelation functions for $n=1$, 4, 5, and 10 illustrating the statistical independence of configurations after ~1 ps.

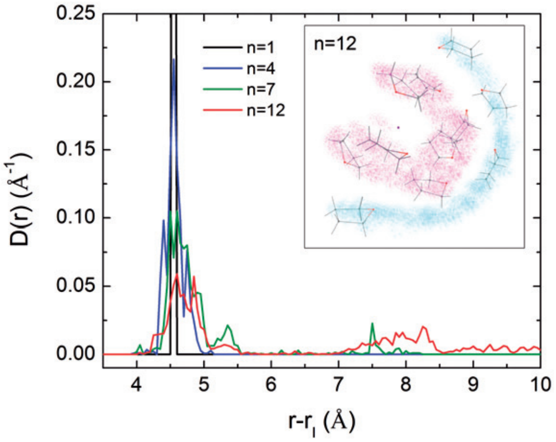

Figure 6. Point dipole distribution $D(r)$ for $n=1$, 4, 7, 12. Inset: Structure of $I^-(THF)_{12}$ with shading highlighting various solvent shells.

quantitative agreement, these results suggest that the AMOEBA structures are qualitatively useful, and should generalize to larger clusters. As a further test, for clusters up to $n=4$, we have taken snapshots from the simulation, relaxed them using the PBE density functional, and compared the resulting VDE's with those calculated at structures relaxed on the AMOEBA potential. As shown in Figure S.1 of the Supplementary material, the resulting VDE versus n curves are essentially parallel to each other.

We use the ensemble of relaxed, phase-space-averaged structures to probe the solvation of iodide in the cluster by computing the solvent radial density for each cluster size. Overall, the relaxed and unrelaxed distribution densities share a very similar solvation trend, including roughly the same coordination numbers, and so we include only the unrelaxed numbers for the sake of brevity. The relaxed radial densities obtained this way for various cluster sizes are shown in Figure 6. For $n=1$, the distribution is centred at about ~4.5 Å and is sharp, suggesting that the structure is relaxing to a single conformation, or a few related structures. Indeed, detailed inspection of the quenched energies suggests that there is just one distinct conformation. By $n=4$, the dipole density shows peaks that are both closer and slightly further from the iodide than the $n=1$ case. Clearly all of the THF molecules are within a first solvent shell for these sizes, reflecting predominance of iodide charge – THF dipole interactions.

Still referring to Figure 6, at $n=7$, the radial density shows an onset of intensity within the interval $r=6.5$–8.5 Å that reflects much larger iodide-THF distances. Integrating $D(r)$ over this region gives 0.45 molecules in this interval, consistent with the emergence of a second solvation layer and thermally-allowed exchanges between configurations that have a 7:0 first-layer-second-layer arrangement and those that have a 6:1 arrangement. Much the same applies to the case of $n=8$, which exhibits 7:1 and 8:0 sets of configurations, and the result of integrating over the intervals we are roughly associating with solvent layers are compiled in Table 2 for $n=1$–14. At $n=9$ and $n=10$, the second layer is more strongly emphasized, with larger average numbers of second-layer THF molecules, though still with only marginal density beyond the second shell. By $n=12$, there is considerable density in both the second layer and what we roughly categorize as a third layer beyond $r=9$ Å. Many different isomeric arrangements appear to be thermally interconvertible at the simulation conditions of 100 K.

We next characterize the nature of the solvation of iodide by THF, which is expected to be somewhere between the well-defined limits of a surface or internal ion, as a function of n. As discussed in the Methods Section, the radius of gyration, Equation (6), is compared against the distance between iodide and the solvent centre of mass. Such a comparison is shown explicitly for $n=4$, 8, and 12 in the curves of Figure 7. From the near-constant value of the radius of gyration at a given n, it is apparent that the cluster is, on average, relatively constant in effective volume (though we cannot rule out fluctuations in components of the radius that are masked in the root mean square). The extent of fluctuations in the relative position of iodide is, on the other hand, visually much larger (~1.5 Å in the case of $n=8$, for instance), and increases with cluster size. For perspective, the case of the relative position superposed on the abscissa would be consistent with full internal solvation, while superposition on

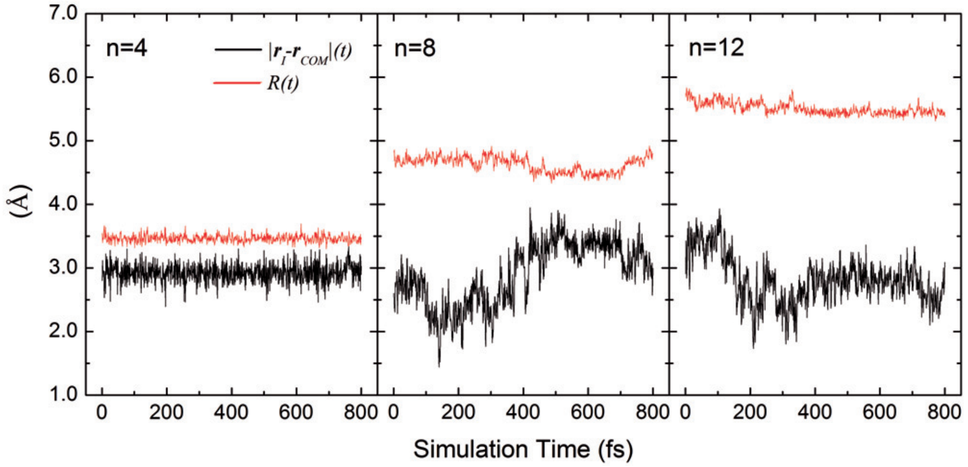

Figure 7. Relative position of iodide, $|r_I - r_{COM}|(t)$, (black), and the cluster radius of gyration, $R(t)$ (red), in simulation time for clusters of $n = 4$, 8, and 12 at 100 K, suggesting a partially-embedded cluster state, with core penetration and cluster radius increasing with cluster size.

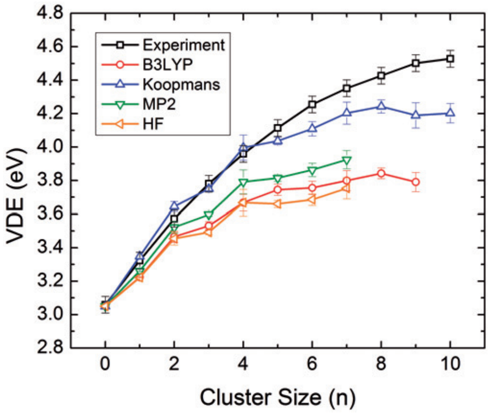

Figure 8. Comparison of the experimental and computational VDE(n).

the radius of gyration would represent an idealized surface state. On this basis, the results from Figure 7 indicate that the iodide lies at or near the cluster surface for $n = 4$ but is partially embedded within the cluster for both $n = 8$ and 12.

The VDEs calculated at the relaxed geometries using various *ab initio* methods are shown graphically in Figure 8, where we have referenced all curves to the experimental VDE of the bare iodide ion to emphasize the comparative trends as a function of cluster size, n. The general trend of increasing stabilization of the anion as a function of n is captured by all the calculations. Both the DFT method, B3LYP, and the wave function approach, MP2, are in near-quantitative agreement with the experimental results out to about $n = 4$, while interestingly, the Koopmans' IPs are in visually better agreement than the more advanced methods for $n = 3$ and beyond. For all methods, however, the slope of the VDE vs n curve is significantly smaller than the experimental result beyond $n = 4$.

For $n = 4$, the three computed lowest-lying singlet-multiplicity (optically-allowed) excited states are very close in energy, with excitation energies of 4.58, 4.59, and 4.61 ± ~0.01 eV and average oscillator strengths ~0.08. The three states' eigenvectors are similar, generally made up of a linear combination of determinants promoting an electron from any one of the set of nearly-degenerate 5 p valence orbitals of iodide (HOMO, HOMO-1, HOMO-2), the degeneracy of which is broken due to the asymmetry of the cluster, to any one of what appear to be Rydberg-type vacant orbitals centred on the solvent molecules (LUMO, LUMO+4, LUMO+8). These orbitals are discussed in Section 4.3. The amplitudes involving these orbital excitations capture ~75% of each of the three excited-state eigenvectors on average, with the 5 p → LUMO excitations carrying the most amplitude (25–35%).

4. Discussion

4.1. *Smaller clusters*

While the location of the iodide cannot be inferred from the photoelectron spectra alone, the spectra do give a great deal of insight into the nature of the stabilization and the infinite size limit. The evolution of the VDEs with cluster size is presented in Figure 3. The VDEs show a significant change in slope at $n = 9$, suggesting that some geometrical structure has been

Table 1. ALMO EDA binding energy components for THF-I$^-$ at various interfragmental distances, THF-I, and equilibrium (THF)$_2$. All values in meV.

Energetic contribution	ΔE_{frz}	ΔE_{pol}	ΔE_{CT}	ΔE_{bind}
Singlet anion, (anion eq., $\lvert r_I - r_O \rvert = 5.6$ Å)	−66	−124	−81	−272
Doublet neutral, (anion eq., $\lvert r_I - r_O \rvert = 5.6$ Å)	58	−2	−52	4
$\Delta(\Delta E)$	124	123	29	276
Singlet anion, second-shell separation $\lvert r_I - r_O \rvert = 8.3$ Å)	−80	−23	−3	−106
(THF)$_2$ ($r_1 - r_2 = 5.2$ Å)	−75	−7	−66	−148

achieved such as a closed solvation shell or a maximization of the coordination number. The rate of change of the VDE, $\Delta E_{stab,}$ is useful in determining the size range of relevant types of ion-solvent interactions. The solvated iodide interacts most strongly with the first 9 THF molecules; after this size the differential stabilization energy drops to only 10–25 meV/molecule. The solvent molecules beyond $n = 9$ only minimally stabilize the charge on the halide, suggesting coordination of the iodide to the solvent cluster is maximized (surface solvation), or possibly due to the closure of the first solvation shell (internal solvation).

The change in the relative interaction values of the solvent and ion at $n = 9$ coincides with an alteration in the shape of the mass spectrum at the same cluster size. The first 9 clusters in the mass spectrum are enhanced relative to the larger cluster sizes, which become about uniform in intensity around $n = 10$. Because the differential stabilization energy is equivalent to the cohesion energy of the cluster (which is related to the enthalpy of evaporation), it is intimately related to the mass spectrum where the larger sizes decay by evaporative loss. When the cluster cohesion energy becomes small, evaporation becomes more probable, leading to the reduction in the measured ion population of those cluster sizes, as is seen in Figure 1 after $n = 9$.

Given the qualitative agreement between the observed and calculated n-dependence of the VDEs for small n (≤ 4) shown in Figure 8, we can use the computations to gain insight into the nature of solvation of the iodide anion in this size regime where the first solvent shell is still incomplete. The starting point is the nature of the interaction between I$^-$ and a single THF molecule, which can be assessed by the ALMO-EDA decomposition presented in Table 1. At the B3LYP level, the $n = 1$ complex is bound by ~270 meV. It is perhaps surprising that only 25% of the binding energy is associated with the frozen orbital term associated with the sum of permanent electrostatics (dominated by charge-dipole interactions) and Pauli repulsions. The predominant fraction (about 45%) of the binding energy arises from electrostatic polarization, and the remaining fraction is due to charge transfer (CT), about 90% of which is due to $5\,p(\mathrm{I}) \rightarrow \sigma^*(\mathrm{CH})$. The critical role for polarization suggests the necessity of using a polarizable force field such as AMOEBA (where of course charge transfer is not explicitly treated). Table 1 also shows that at a separation of ~8 Å, characteristic of the second solvation shell, 83% of the ~100 meV I$^-$(THF) binding energy originates from frozen electrostatics, and the polarization contribution is relatively small.

When the same decomposition analysis is performed on the doublet surface of the detached species evaluated vertically, the effect of the excess valence electron on the interaction can be revealed by the differences in each component of the binding energy, which are shown in the row of Table 1 labelled as $\Delta(\Delta E)$. There is a nearly equivalent loss of frozen and polarization interactions upon ionization. The fact that polarization is reduced to nearly zero is consistent with intuition. By contrast, the fact that frozen interactions are repulsive in the neutral species reveals the role of Pauli repulsions at the anion geometry, which are expected to be of at least this magnitude. Accordingly, the permanent charge-dipole interaction is at least 124 meV in the anion. It also shows that the effective van der Waals radii of the iodine atom and anion are quite similar, as anticipated based on elementary shell filling and screening arguments. The charge-transfer interaction between neutral I and THF is roughly equally divided between forward $5p(\mathrm{I}) \rightarrow \sigma^*(\mathrm{CH})$ donation and back donation which now becomes possible from filled solvent CH orbitals into the empty I 5 p orbital. The considerable magnitude of the CT interaction for neutral iodine is noteworthy. Finally we note that of course the optimized neutral geometry (not evaluated here) may differ considerably from the anion geometry.

The connection between the observed VDEs and the n-dependent 100 K solvation dynamics obtained as AMOEBA trajectories can be assessed from Figure 3 and Figure 6 together with Table 2. From the table, we note that population of a second layer commences around $n = 7$, with a calculated average of 0.45 solvent

Table 2. Solvation layers about iodide given by integration of the relaxed $D(r)$.

	Integrated intensity within a range for $|r_I - r_O|$:		
Cluster size	1.95–6.45 Å	6.50–8.95 Å	9.00–16.00 Å
$n = 1$	1	0	0
2	2	0	0
3	3	0	0
4	4	0	0
5	5	0	0
6	6	0	0
7	6.55	0.45	0
8	7.46	0.54	0
9	6	2.8	0.2
10	6	3.9	0.1
11	7	4	0
12	6.92	3.6	1.48
13	8	4.984	0.016
14	8.83	3.05	2.12

molecules in the second layer, meaning a distribution of 7:0 and 6:1 structures (and possibly 5:2 ones, etc). Similar results are seen at $n = 8$. By $n = 9$, an average of 2.8 molecules are associated with a second layer, and a small population is also evident in what may be roughly identified as a third layer. Thus there is evidence from the trajectories of a closing of the first solvent shell around 8–9 THF molecules, which is in very good agreement with the experimental evidence discussed above. However, the non-integer number of second layer atoms reported in Table 2 reflects the fact that there are many of local minima which include many different arrangements of first and second layers of solvent molecules. Thus, there is not a sharp shell closing as a function of n in the 100 K trajectories, but rather a gradual shift to an increasing fraction of sampled geometries which include one or more second layer molecules.

The comparison between theory and experiment cannot be considered fully satisfactory, however, as the calculated VDE's, based on the geometries that gave rise to the analysis above, do not show a similar transition in differential stabilization around $n = 9$. Instead, the calculated VDE's turn over much sooner, at approximately $n = 4$. The most likely origin of this discrepancy is some deviation between the AMOEBA potential energy surface for the anionic clusters and the true *ab initio* surfaces. Some evidence for this arises from the difference discussed in the Methods section for the geometry of the $n = 1$ complex, where *ab initio* methods prefer more compact THF-iodide distances. However, DFT-based relaxations of the AMOEBA geometries of the clusters up to $n = 4$ as shown in Figure S.1 of the Supplementary material do not lead to significant differences in the calculated VDEs. To resolve this issue, it would be useful to revisit iodide-THF simulations with fully *ab initio* methods in the future.

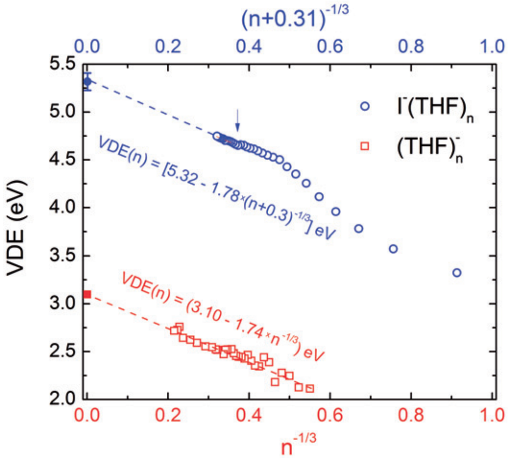

Figure 9. VDE vs. $(n+\xi)^{-1/3}$ for $I^-(THF)_n$ (blue circles) and $(THF)_n^-$ (red squares), adapted from Young *et al*. [20]. For iodide, $\xi = 0.3$, while for $(THF)_n^-$ $\xi = 0$. Linear fits are shown next to each data set. The similarity in the slopes indicates the same stabilizing interaction.

4.2. *Larger clusters*

For larger clusters ($n > 15$), there are no calculated structures for direct comparison, so we appeal to classical electrostatic models to interpret the experimental results. Motivated by dielectric continuum models where the ion is treated as a hard sphere within a uniform dielectric sphere [50–52], the VDEs are plotted in Figure 9 against the inverse cluster radius, $(n+\xi)^{-1/3}$, where ξ is the ratio of the ion volume to the molecular volume. The VDEs for bare THF cluster anions, $(THF)_n^-$, are also shown in the figure. Using the hard-sphere ionic radius of iodide (216 pm) and the room-temperature density of THF to estimate its molar volume, ξ is approximately 0.3. Fitting the linear region of the $I^-(THF)_n$ plot yields an estimate of the bulk VDE of I^- in THF (intercept) and the nature of the stabilization with increasing cluster size (slope). A close examination of Figure 9 shows a second kink in the linear region, this time around $n = 19$, where the slope of the line increases. Fitting only this region ($19 \leq n \leq 30$) yields:

$$VDE(n) = [5.32 - 1.78(n+0.3)^{-1/3}]\ \text{eV} \qquad (10)$$

Fitting the entire linear range results in a lower slope (-1.47 ± 0.03 eV) but a similar intercept (5.2 ± 0.1 eV). At sufficiently large cluster sizes, the charge will still be

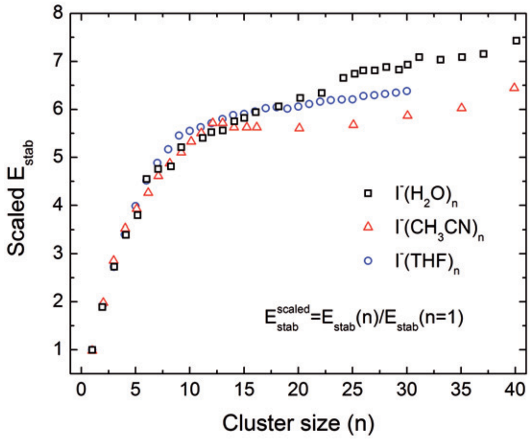

Figure 10. Scaled differential stabilization energy for iodide in water (black squares), acetonitrile (red triangles), adapted from Markovitch *et al.* [11], and THF (blue circles).

stabilized by additional solvent molecules, however the influence of the anion on solvent packing and structure will decrease, similarly to the case for a solvated electron [20]. Comparing the slopes of the larger $I^-(THF)_n$ VDEs (-1.78 ± 0.06 eV) to that of the $(THF)_n^-$ (-1.74 ± 0.09 eV) shows that the nature of the stabilization is very similar, i.e. driven by long-range interactions. This similarity would indicate that around $n = 9$ the specific nature of the excess charge, such as its shape or general size, is unimportant to how the clusters electrostatically stabilize the charge, with this effect becoming even less significant by $n = 19$. For instance, the radius of gyration for solvated electrons in THF is ~4 Å [53], while the ionic radius of iodide is about half that. The linear extrapolation gives an approximation of the bulk binding energy of iodide in THF of about 5.3 ± 0.1 eV, indicating a stabilization energy of 2.24 eV at infinite cluster size. The degree of stabilization is substantially different than that of iodide in water or acetonitrile where the ion is stabilized by about twice as much (4.6–4.8 eV) [11] but is similar to solvation in xenon clusters (1.4 eV) [13]. Like THF, xenon has no organized bonding network to disrupt, but the strong dipole of THF should lead to some enhanced stabilization not afforded by the Xe atoms. Some insight can be gained by comparing these above inferences to systems where the location of iodide is better established. Comparing the absolute stabilization energies for each solvent is difficult because the nature of the interactions differs vastly for each molecule (THF, for instance, is incapable of hydrogen bonding). Therefore, a common energy scale must be established. This is done by scaling the stabilization energy of each solvent by the value of the iodide–solvent monomer interaction [11]:

$$Scaled\ E_{stab}^{(solvent)}(n) = E_{stab}^{(solvent)}(n)/E_{stab}^{(solvent)}(n=1) \quad (11)$$

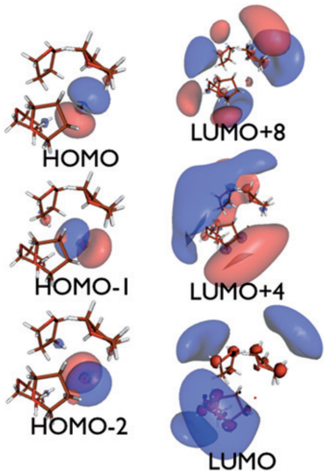

Figure 11. Excited states for $n = 4$. The diffuse and solvent-centred nature of the wavefunction suggests the excited state is a 'charge-transfer-to-solvent' state.

This is shown in Figure 10 for iodide in THF, water and acetonitrile, with the latter two solvent values adapted from Markovich *et al.* [11]. The partially-embedded nature of iodide in THF places it between the two limiting cases of water and acetonitrile for surface and internal solvation, respectively. In water, iodide may still reside on the cluster surface while the VDEs continue to rise until $n \sim 60$. In contrast, the closure of the first solvation shell in acetonitrile results in a loss of differential stabilization energy after $n = 12$; the VDE vs. cluster size curve is flat for larger sizes. Indeed this type of 'intermediate' stabilization is reflected in the structures, as the partially-embedded location of the iodide in THF clusters shares some aspects of surface- and internal-solvation.

4.3. *Excited states*

Excited state orbitals of $I^-(THF)_4$ are plotted in Figure 11. The signal at low eKE in Figure 4 at an excitation energy of 4.05 eV is a signature resonant excitation to the cluster analog of a charge-transfer-to-solvent (CTTS) state [54]. This feature results from excited state autodetachment, in which the photo-excited cluster, approximated as $I{\cdot}(THF)_n{}^-$ (see LUMO in Figure 11), decays by ejection of a very slow electron [47]. As the cluster size is increased from $n = 4$–8, the autodetachment signal becomes less intense and narrower. This trend suggests that the adiabatic detachment energy increases more rapidly with cluster size than the CTTS transition energy, effectively halting excitation of the CTTS state and subsequent autodetachment once the entire CTTS band lies below the adiabatic detachment energy. Similar results were seen for iodide-doped water clusters [55] where the autodetachment channel closes by $n = 15$ and the resultant water cluster anions are adiabatically stable at that size range [56]. In contrast, methanol cluster anions [57] are not stable below $n \sim 70$, causing the $\mathrm{I}^-(\mathrm{CH_3OH})_n$ clusters to have vastly reduced excited state lifetimes [58].

The calculated excited-state roots are between 660 and 690 meV above the value for detachment to the continuum (VDE/B3LYP = 3.92 eV) for $n = 4$. This is qualitatively consistent with the experimental result, and therefore the vibrational auto-detachment feature is attributable to the metastability of the vertically-excited anionic species. Given the experimental observation of differential stabilization of the anion ground state by over 400 meV at $n = 8$ relative to $n = 4$, it is likely that the lowest excited state will become bound in that same size regime.

5. Conclusions

Using photoelectron imaging and electronic structure theory, we have investigated the solvation of iodide in tetrahydrofuran clusters. For clusters larger than $n = 9$, the VDEs begin to level out as the iodide ion appears coordinated to 7–9 THF molecules, embedded toward the surface of the cluster but not fully solvated. After $n = 9$, solvent-solvent stacking begins. A metastable electronic excited state is seen in experiments in clusters of as few as 4 THF molecules, with the excited state autodetachment channel closing by $n = 8$. This indicates the clusters can readily accept the electron and excess energy after electron transfer, as suggested by the nature of anionic THF clusters, $(\mathrm{THF})_n^-$. More experimental work is needed to understand the dynamics of electron transfer in these clusters and is currently underway in our laboratory. Infrared studies on both the iodide-doped and negative ions of THF clusters would be very useful in understanding the nature of charge/ion stabilization for this solvent. Moreover, these studies lay the groundwork for the development of a detailed, molecular-level picture of the charge-transfer-to-solvent dynamics in THF clusters.

Acknowledgements

D.M.N. acknowledges support by the U.S. National Science Foundation (NSF) (CHE-0649647) and M.H.G. acknowledges support from U.S. Department of Energy under Contract No. DE-AC02-05CH11231. The authors are grateful to Chen Zhao for acquiring dry THF, Paul Horn for access to the unrestricted ALMO code, and Samuel Fenton Manzer for computational scripts.

References

[1] X. Chen and S.E. Bradforth, Annu. Rev. Phys. Chem. **59**, 203 (2007).
[2] W.H. Robertson and M.A. Johnson, Annu. Rev. Phys. Chem. **54**, 173 (2003).
[3] P. Jungwirth and D.J. Tobias, J. Phys. Chem. B **106**, 6361 (2002).
[4] B. Winter, R. Weber, I.V. Hertel, M. Faubel, P. Jungwirth, E.C. Brown and S.E. Bradforth, J. Am. Chem. Soc. **127**, 7203 (2005).
[5] A.W. Castleman Jr and K.H. Bowen Jr, J. Phys. Chem. **100**, 12911 (1996).
[6] D.M. Koch and G.H. Peslherbe, Chem. Phys. Lett. **359** (5–6), 381 (2002).
[7] M.J. Blandamer and M.F. Fox, Chem. Rev. **70** (59), 59 (1970).
[8] G. Markovich, S. Pollack, R. Giniger and O. Cheshnovsky, J. Chem. Phys. **101** (11), 9344 (1994).
[9] G. Markovich, S. Pollack, R. Giniger and O. Cheshnovsky, Z. Phys. D **26**, 98 (1993).
[10] C.E.H. Dessent, C.G. Bailey and M.A. Johnson, J. Chem. Phys. **103** (6), 2006 (1995).
[11] G. Markovich, L. Perera, M.L. Berkowitz and O. Cheshnovsky, J. Chem. Phys. **105** (7), 2675 (1996).
[12] T. Takayanagi, J. Phys. Chem. A **110** (22), 7011 (2006).
[13] I. Becker and O. Cheshnovsky, J. Chem. Phys. **110** (13), 6288 (1999).
[14] I. Becker, G. Markovich and O. Cheshnovsky, Phys. Rev. Lett. **79** (18), 3391 (1997).
[15] M.T. Zanni, C. Frischkorn, A.V. Davis and D.M. Neumark, J. Phys. Chem. A **104** (12), 2527 (2000).
[16] M.J. Bedard-Hearn, R.E. Larsen and B.J. Schwartz, J. Chem. Phys. **122**, 134506 (2005).
[17] D.T. Bowron, J.L. Finney and A.K. Soper, J. Am. Chem. Soc. **128**, 5119 (2006).
[18] I.B. Martini, E.R. Barthel and B.J. Schwartz, Science **293** (5529), 462 (2001).
[19] A.E. Bragg and B.J. Schwartz, J. Phys. Chem. B **112**, 483 (2008).
[20] R.M. Young, M.A. Yandell, M. Niemeyer and D.M. Neumark, J. Chem. Phys. **133** (15), 154312 (2010).
[21] Alexander T. Shreve, Madeline H. Elkins, and D.M. Neumark. Private Communication.
[22] A.V. Davis, R. Wester, A.E. Bragg and D.M. Neumark, J. Chem. Phys. **118** (3), 999 (2003).
[23] U. Even, J. Jortner, D. Noy, N. Lavie and C. Cossart-Magos, J. Chem. Phys. **112** (18), 8068 (2000).
[24] W.C. Wiley and I.H. McLaren, Rev. Sci. Instrum. **26** (12), 1150 (1955).
[25] A.T.J.B. Eppink and D.H. Parker, Rev. Sci. Instrum. **68** (9), 3477 (1997).
[26] V. Dribinski, A. Ossadtchi, V.A. Mandelshtam and H. Reisler, Rev. Sci. Instrum. **73** (7), 2634 (2002).

[27] T. Andersen, H.K. Haugen and H. Hotop, J. Phys. Chem. Ref. Data **28** (6), 1511 (1999).

[28] Y. Shao, L.F. Molnar, Y. Jung, J. Kussmann, C. Ochsenfeld, S.T. Brown, A.T.B. Gilbert, L.V. Slipchenko, S.V. Levchenko, D.P. O'Neill, R.A. DiStasio Jr, R.C. Lochan, T. Wang, G.J.O. Beran, N.A. Besley, J.M. Herbert, C. Yeh Lin, T. Van Voorhis, S. Hung Chien, A. Sodt, R.P. Steele, V.A. Rassolov, P.E. Maslen, P.P. Korambath, R.D. Adamson, B. Austin, J. Baker, E.F.C. Byrd, H. Dachsel, R.J. Doerksen, A. Dreuw, B.D. Dunietz, A.D. Dutoi, T.R. Furlani, S.R. Gwaltney, A. Heyden, S. Hirata, C.-P. Hsu, G. Kedziora, R.Z. Khalliulin, P. Klunzinger, A.M. Lee, M.S. Lee, W. Liang, I. Lotan, N. Nair, B. Peters, E.I. Proynov, P.A. Pieniazek, Y. Min Rhee, J. Ritchie, E. Rosta, C. David Sherrill, A.C. Simmonett, J.E. Subotnik, H. Lee Woodcock Iii, W. Zhang, A.T. Bell, A.K. Chakraborty, D.M. Chipman, F.J. Keil, A. Warshel, W.J. Hehre, H.F. Schaefer Iii, J. Kong, A.I. Krylov, P.M.W. Gill and M. Head-Gordon, Phys. Chem. Chem. Phys. **8** (27), 3172 (2006).

[29] A.D. Becke, J. Chem. Phys. **98** (7), 5648 (1993).

[30] J.P. Perdew, K. Burke and M. Ernzerhof, Phys. Rev. Lett. **78** (7), 1396 (1997).

[31] K.A. Peterson, B.C. Shepler, D. Figgen and H. Stoll, J. Phys. Chem. A **110** (51), 13877 (2006).

[32] D.J. Tozer and N.C. Handy, J. Chem. Phys. **109** (23), 10180 (1998).

[33] J. Häsing, Annalen der Physik **429** (7), 509 (1940).

[34] J.M. Herbert and M. Head-Gordon, Proc. Nat. Acad. Sci. USA **103** (39), 14282 (2006).

[35] J.-D. Chai and M. Head-Gordon, J. Chem. Phys. **128** (8), 084106 (2008).

[36] J.-D. Chai and M. Head-Gordon, Phys. Chem. Chem. Phys. **10** (44), 6615 (2008).

[37] J.W. Ponder, *TINKER: Software Tools for Molecular Design* (Washington University, St. Louis, MO, 2011).

[38] J.W. Ponder, C. Wu, P. Ren, V.S. Pande, J.D. Chodera, M.J. Schnieders, I. Haque, D.L. Mobley, D.S. Lambrecht, R.A. DiStasio, M. Head-Gordon, G.N.I. Clark, M.E. Johnson and T. Head-Gordon, J. Phys. Chem. B **114** (8), 2549 (2010).

[39] G. Pfafferott, H. Oberhammer, J.E. Boggs and W. Caminati, J. Am. Chem. Soc. **107** (8), 2305 (1985).

[40] S.J. Stuart and B.J. Berne, J. Phys. Chem. **100** (29), 11934 (1996).

[41] R.Z. Khaliullin, E.A. Cobar, R.C. Lochan, A.T. Bell and M. Head-Gordon, J. Phys. Chem. A **111** (36), 8753 (2007).

[42] R.Z. Khaliullin, M. Head-Gordon and A.T. Bell, J. Chem. Phys. **124** (20), 204105 (2006).

[43] R.Z. Khaliullin, A.T. Bell and M. Head-Gordon, J. Chem. Phys. **128** (18), 184112 (2008).

[44] D.H. Ess, W.A. Goddard and R.A. Periana, Organometallics **29** (23), 6459 (2010).

[45] J.M.J. Swanson and J. Simons, J. Phys. Chem. B **113** (15), 5149 (2009).

[46] E. Ramos-Cordoba, D.S. Lambrecht and M. Head-Gordon, Faraday Disc. **150** (0), 345 (2011).

[47] A. Kammrath, J.R.R. Verlet, A.E. Bragg, G.B. Griffin and D.M. Neumark, J. Phys. Chem. A **109**, 11475 (2005).

[48] O.T. Ehrler, G.B. Griffin, R.M. Young and D.M. Neumark, J. Phys. Chem. B **113**, 4031 (2009).

[49] R.M. Young, M.A. Yandell and D.M. Neumark, J. Chem. Phys. **134** (12), 124311 (2011).

[50] R.N. Barnett, U. Landman and C.L. Cleveland, Chem. Phys. Lett. **145** (5), 382 (1988).

[51] G. Makov and A. Nitzan, J. Phys. Chem. **98** (13), 3459 (1994).

[52] R.D. Levine, *Molecular Reaction Dynamics* (Cambridge University Press, Cambridge, United Kingdom, 2005).

[53] W. Marbach, A.N. Asaad and P. Krebs, J. Phys. Chem. A **103**, 28 (1999).

[54] D. Serxner, C.E.H. Dessent and M.A. Johnson, J. Chem. Phys. **105** (16), 7231 (1996).

[55] J.R.R. Verlet, A. Kammrath, G.B. Griffin and D.M. Neumark, J. Chem. Phys. **123** (231102), 4 (2005).

[56] J.R.R. Verlet, A.E. Bragg, A. Kammrath, O. Cheshnovsky and D.M. Neumark, Science **307**, 93 (2005).

[57] A. Kammrath, J.R.R. Verlet, G.B. Griffin and D.M. Neumark, J. Chem. Phys. **125**, 171102 (2006).

[58] M.A. Yandell, R.M. Young, S.B. King and D.M. Neumark, J. Phys. Chem. A **116**, 2750 (2011).